

# Artificial Phototropic Systems for Enhanced Light Harvesting Based on a Liquid Crystal Elastomer

Yichen Yan, Yusen Zhao, Yousif Alsaïd, Bowen Yao, Yucheng Zhang, Shuwang Wu, and Ximin He\*

Oblique-incidence-induced energy-density loss (OEL) is a universal problem which affects nearly all processes involving electromagnetic waves, especially sunlight harvesting. Technologies (solar concentrating plants, large scale systems, etc.) are developed to address this issue, albeit with limitations such as complex design, large size, and high cost. Inspired by nature, artificial phototropism is developed to accurately follow the light direction without complex motors system and electrical control. However, the existing systems are limited by small tracking operation windows, low robustness, or the requirement of high-power input. Herein, a system is reported that is versatile, low cost, mechanically strong, and can achieve large-angle reorientation driven by unconcentrated sunlight. This system is demonstrated to be able to recover the OEL for photovoltaics as well as solar vapor generation (SVG) processes. Compared with the nonphototropic system, it can achieve 447% output in lab and 155% in real-life applications. The principle behind our artificial phototropic system is universal and can be extended to many optical applications, especially sunlight harvesting.

## 1. Introduction

Many plants in nature developed phototropism, the ability to not only detect the sunlight direction, but also automatically and constantly follow the light from sunrise to sunset. This directional locomotion is achieved by the self-regulation of plants inherently between their bodies and light stimulus. For plants, developing phototropism allows for the recovery of oblique-incidence

energy-density loss (OEL),<sup>[1]</sup> whereby, for instance, the energy density of light can be greatly reduced by 50% at 60° incidence angle (the angle between the light ray and the surface normal). As a result, continually tracking sunlight allows more energy to be acquired from the sun to benefit the well-being and proliferation of plants.<sup>[2]</sup> In addition to plant growth, OEL as a universal problem also influences all energy harvesting processes involving electromagnetic waves, during which the receiving plane of optical/optochemical/optomechanical/optoelectronic devices is not normal to the light beam (Figure 1). For a device which can recover the OEL, 400% enhancement could be achieved compared with the nontropic analog.<sup>[1]</sup> Several current technologies have been developed to address the OEL, albeit with limitations. Motionless designs, such as microstructure in poly(methyl methacrylate),<sup>[3,4]</sup> can redi-

rect sunlight without moving parts, simplifying the system. However, as the incidence angle changes, the angle between the redirected light and the receiving plane will also change. Therefore, it can only achieve normal incidence of light in very limited incidence light angle window. Moreover, the addition of materials in front of the receiving plane will result in extra light reflection and absorption loss. Designs based on electronically controlled motors to move the receiving plane such as Smartflower,<sup>[5]</sup> Solar Sunflower,<sup>[6]</sup> and solar concentration dishes can accurately track sunlight regardless of incidence angle; in addition, the exclusion of excess materials in front of the receiving plane benefits the efficiency. However, the requirement of additional mechanics in the design increases their complexity and cost. Large-scale solar power concentration plants (e.g., Gemasolar<sup>[7]</sup> and Ivanpah<sup>[8]</sup>) also require extremely large space (hundreds to thousands acres) to construct an electronically controlled mechanism to suitably track and orient toward sunlight. A simpler system is thus highly desired, preferably using bioinspired artificial phototropism without electronics, to fully utilize the potential of OEL recovery to boost the performance of optical and electromagnetic devices.

Artificial phototropism has been studied, with the overarching goal of tracking high incidence angle light, functioning in low light intensity, and offering the capability to integrate additional optical devices; such characteristics enable artificial phototropism in a broad range of applications. Li et al. reported an

Y. Yan, Y. Zhao, Y. Alsaïd, Dr. B. Yao, Y. Zhang, Dr. S. Wu, Dr. X. He  
Department of Materials Science and Engineering  
University of California  
Los Angeles, CA 90095, USA  
E-mail: ximinhe@ucla.edu

Dr. B. Yao, Dr. S. Wu  
School of Chemistry and Chemical Engineering  
State Key Laboratory of Metal Matrix Composites  
Shanghai Jiao Tong University  
800 Dongchuan Road, Shanghai 200240, China

 The ORCID identification number(s) for the author(s) of this article can be found under <https://doi.org/10.1002/aisy.202000234>.

© 2021 The Authors. Advanced Intelligent Systems published by Wiley-VCH GmbH. This is an open access article under the terms of the Creative Commons Attribution License, which permits use, distribution and reproduction in any medium, provided the original work is properly cited.

DOI: 10.1002/aisy.202000234

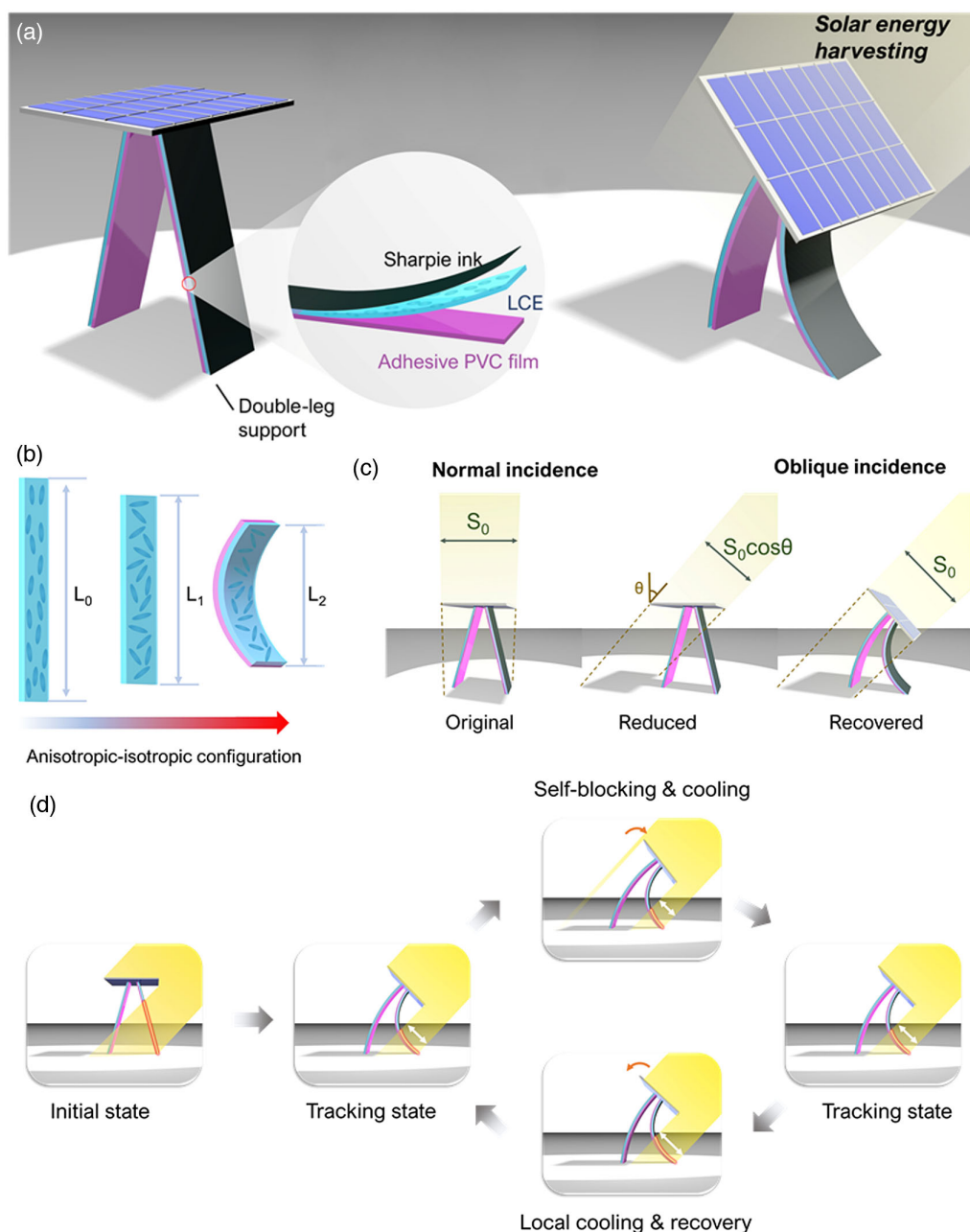


**Figure 1.** a) Schematic illustration of the general design of the phototropic system based on LCE. b) Illustration of the LCE configuration change and bimorph design. c) Illustration of OEL. d) Illustration of the feedback loop.

actuator system based on carbon nanotubes (CNTs) and thermoresponsive liquid crystal elastomer (LCE).<sup>[9]</sup> The system is able to tilt the solar panel on top toward the light direction, albeit with a limited bending angle ( $<20^\circ$ ) under 1 sun intensity ( $1000 \text{ W m}^{-2}$ ). In addition, the light concentrator and heat collector add capital cost and complexity to the design. Shape-memory alloys, thermoresponsive springs, and lenses systems have also been demonstrated.<sup>[10]</sup> However, they still suffer from a limited bending angle, complex optomechanical design, and undesirable integration of bulky optical lenses. Recently, Qian et al. for the

first time demonstrated an omnidirectional light tracker at 1 sun enabled by a built-in feedback loop, with thermoresponsive poly(*N*-isopropylacrylamide) (PNIPAM) hydrogels containing reduced graphene oxide (rGO) or gold nanoparticles (AuNP), which can achieve high incident-angle light tracking.<sup>[11]</sup> However, the hydrogel materials used in this work are mechanically weak to self-stand in air and support additional optical devices if held on top of them. Single LCE pillars and liquid-vapor phase transition phototropic actuators have been reported for wide tracking operation windows, but limited by the high-power,

laser-driven requirement that exceeds the intensity of that specific wavelength in the solar spectrum.<sup>[11,12]</sup> Therefore, it is highly desirable to develop a simple, low-cost intelligent system that can utilize sunlight (at or lower than  $1000 \text{ W m}^{-2}$ ) to achieve large-angle phototropic reorientation while remaining mechanically strong enough to support and drive optical devices.

Herein, we demonstrate an LCE-based phototropic material system, which meets these criteria and can be applied for enhancing the light harvesting and thus the performance of various optical devices such as solar cells and solar vapor generation (SVG) at oblique sunlight illumination. This system utilizes the LCE bimorph structure as legs in a double-leg design to support the optical devices on top to achieve large actuation and high load-bearing ability. Driven by unconcentrated sunlight ( $700\text{--}1000 \text{ W m}^{-2}$ ), the system can achieve bending angles over  $60^\circ$  with a fast response (40 s) and reversible recovery to the original vertical position. The bimorph structure of the LCE and passive layer improves the deformation. The double-leg design enables self-standing, with the ability to support additional loads on top of the device. The use of common stationery (Sharpie marker pen and 3 M tape) and off-the-shelf ingredients reduces the cost of fabrication significantly. We have demonstrated this design can be used to recover the OEL in solar-to-electricity conversion as well as SVG processes. With its load-bearing ability, this device is promising for optical and electromagnetic applications such as satellite solar energy capture and self-aligned light communication (light fidelity, LiFi).

## 2. Result and Discussion

### 2.1. System Design

Figure 1a shows the general design of the device using an LCE/tape bimorph actuator featuring double-leg support. Liquid crystals are chosen for being tougher than hydrogels and able to generate larger forces, increasing the load-bearing ability of the device. They can also be made thermoresponsive, allowing for photothermal actuation with the inclusion of a photothermal absorber. In addition, they allow the design of the feedback loop in the system. To render the LCE thermoresponsive, it is mechanically aligned and then cross-linked to form an elastomer with length  $L_0$  (Figure 1b). When heated, the molecular alignment in the LCE will convert to a random orientation, leading to a decreased macroscopic length ( $L_1$ ) and an increase in width (Figure 1b,  $L_1$  and Figure S1a, Supporting Information). The LCE length contraction can lead to bending with the addition of a nonthermoresponsive PVC tape to form a bimorph structure. The bending originates from the difference in length of the two adhered layers (Figure 1b,  $L_2$ ; Figure S1b, Supporting Information). Note that the small contraction ratio is sufficient to trigger large bending deformation, which amplifies the actuation under the same light input.<sup>[13,14]</sup> The bimorph proposed here can respond to light in a broad temperature range (Figure S2 and S3, Supporting Information) of  $5\text{--}50^\circ\text{C}$ , rendering the system the ability to adapt various working environments.

In addition to the bimorph structure, the double-leg support is another factor that contributes to the high load-bearing ability and the large actuation range of the system. As opposed to

the single-leg design previously reported,<sup>[1]</sup> the double-leg design was used for its high load-bearing capability benefiting from the good stability of its triangle shape. However, such a design would compromise the extent of actuation, limiting the maximum bending angle and consequently the amount of light recovery. Introducing the bimorph can effectively enhance the actuation ability and alleviate the problem. The correlation between the phototropic device dimensions, mechanics, and tracking performance has been discussed (Figure S4–S6, Supporting Information). Double-leg support and bimorph work synergistically realize the desirable high load-bearing ability and large actuation range, provided the distance between the legs at the bottom is carefully optimized (Figure S7, Supporting Information).

To make the thermoresponsive LCE able to respond to light, marker pen ink is directly applied on the LCE surface and used as the photothermal converter, a low-cost alternative to previously studied CNTs, rGOs, AuNPs, and so on. The use of these materials usually involves premixing in the LCE precursors, rather than fabricate a film on the LCE surface, to circumvent the delamination issue, which potentially will result in problems in the photocross-linking of the aligned molecule networks due to their light-absorbing abilities. Ink, on the contrary, can be directly applied onto the surface of the LCE without delamination. In addition, some of these particles, such as CNT, experience solubility issues in the toluene-based LCE precursors. The use of marker pen ink avoids the cross-linking and solubility issues while also exhibiting suitably high light absorption. As indicated in the UV-vis spectroscopy (Figure S8, Supporting Information), inked LCE demonstrates very low reflectance for  $250\text{--}1500 \text{ nm}$  light. Transmittance of  $250\text{--}800 \text{ nm}$  is also very low, with small rise in transmittance in the infrared (IR) region. Because the transmittance and reflectance are very low, light of  $250\text{--}800 \text{ nm}$  can be considered largely absorbed by the ink-coated LCE. Given that most of the energy in the solar spectrum is in this region,<sup>[15]</sup> this result indicates that the marker pen ink is suitable for use as the photothermal converter.

A negative feedback loop<sup>[1]</sup> (Figure 1d) is inherently formed from the light-material interaction, which autonomously regulates the bending angle of the LCE and enables its accurate self-orientation toward light. This feedback loop will eventually let the system oscillate around the exact angle of the incident light and reach steady alignment eventually, regardless of the light direction. In the initial state, the system stands vertically. Upon illumination, the system will actuate toward the light source due to asymmetric heating of the two legs. As the bending angle increases, a smaller area of the LCE surface will be illuminated by light due to the self-shadowing. When the system reaches the light angle, the LCE surface will be in the shadows, which results in the cooling of the LCE and the tendency to return to the initial vertical state. However, such a recovery will lead to the diminishing of the self-blocking effect. As a result, the system will be kept at this bending state with small oscillation, which will reach a dynamic equilibrium state of aiming. Such a built-in feedback loop ensures the system orientation can accurately point toward the incident light direction with a minute oscillation around the equilibrium position (Movie S1, Supporting Information); this largely increases the light recovering ability.

In comparison with the LCE/tape photothermal conversion system in this work, azobenzene-based material systems can also

achieve light-triggered actuation without the need for a photothermal absorber, enabling a simpler design; however, to revert to the original state, the azobenzene system requires excitation from another specific wavelength (different from the one used to trigger the initial actuation) or thermally driving it back in the dark.<sup>[16–19]</sup> Such a requirement makes it difficult to design the feedback loop using a simple setup. An azobenzene design is therefore not a suitable alternative to the photothermally actuated LCE design for achieving a reversible feedback loop with accurate light tracking.

## 2.2. Phototropism of the Solar Panel Phototropic Device

To demonstrate the system's ability to reorient toward light and recover the OEL, solar panels were mounted on the top of the phototropic device. Light generated by a solar simulator of various intensities ( $700\text{--}1000\text{ W m}^{-2}$ ,  $0.7\text{--}1.0$  sun) and various incidence angles ( $30^\circ$ ,  $45^\circ$ , and  $60^\circ$ ) was used to test the final equilibrium bending angle of the phototropic device (Figure 2b). At  $30^\circ$  and  $45^\circ$ , the device showed remarkable tracking performance, able to accurately reorient itself toward sunlight with an error of less than  $0.2^\circ$  even at  $900\text{ W m}^{-2}$  intensity (lower than 1 sun). At a  $60^\circ$  incidence angle, it could bend to  $53^\circ$  and  $57^\circ$  final angle at  $700$  at  $1000\text{ W m}^{-2}$  intensity, respectively; this still represents significantly improved tracking performance, considering 99.86% (for  $57^\circ$  final angle) of light is recovered compared with its vertical position. It could also bend under natural sunlight condition (Movie S2, Supporting Information), where the intensity is less than  $1000\text{ W m}^{-2}$ . The phototropic device not only accurately reorients itself toward light, but also does so in a prompt manner. At the  $60^\circ$  and  $45^\circ$  incidence angles (Figure 2c,d, respectively), it can reorient itself from a vertical position to the final bending state within 40 s, regardless the light intensity. Interestingly, during the phototropic bending process,

the device first showed a sharp increase in its bending angle followed by a slow bending backward to the final bending state. Such a phenomenon is believed to come from the momentum on the load (solar panel) sitting on top of the system: during the bending process (Figure 2a), the movement of the legs causes the reorientation of the solar panel, which provides the momentum contributing to the overshoot of final equilibrium bending state. After that, the motion of the solar panel is restricted by the LCE legs. Finally, the system reaches its dynamic equilibrium state, and a steady final bending angle can be recorded. Fine-tuning the load weight of the phototropic device can influence the fast bending as well as the overshoot behavior, as both will cease to exist if the load weight is reduced to  $2/3$  of the optimized weight. At a  $30^\circ$  incident angle (Figure 2e), the device took about 90 s to reach its final bending state, and a spike of the bending angle was not observed. This could be because the relatively little motion of the  $30^\circ$  reorientation cannot provide enough momentum for the solar panel, and the legs experience less power density at the small incident angle.

## 2.3. OEL Recovery of the Solar Panel Phototropic Device

The OEL recovery ability of the phototropic device is also tested by recording the  $I\text{--}V$  curves from the solar panels (see Experimental Section) mounted on top and comparing with a nonphototropic control (stationary solar panel in horizontal position), recorded for  $1000\text{ W m}^{-2}$  light with an angle of  $60^\circ$ ,  $45^\circ$ , and  $30^\circ$  (Figure 3a–c, respectively). At all voltages, the phototropic device can output up to 200% current, indicating that it is able to deliver more energy compared with the nonphototropic control. The maximum power output is calculated from the  $I\text{--}V$  curve data by multiplying the current with the respective voltage and finding the largest value. The maximum output power of the solar panel is also calculated for  $60^\circ$  light illumination and

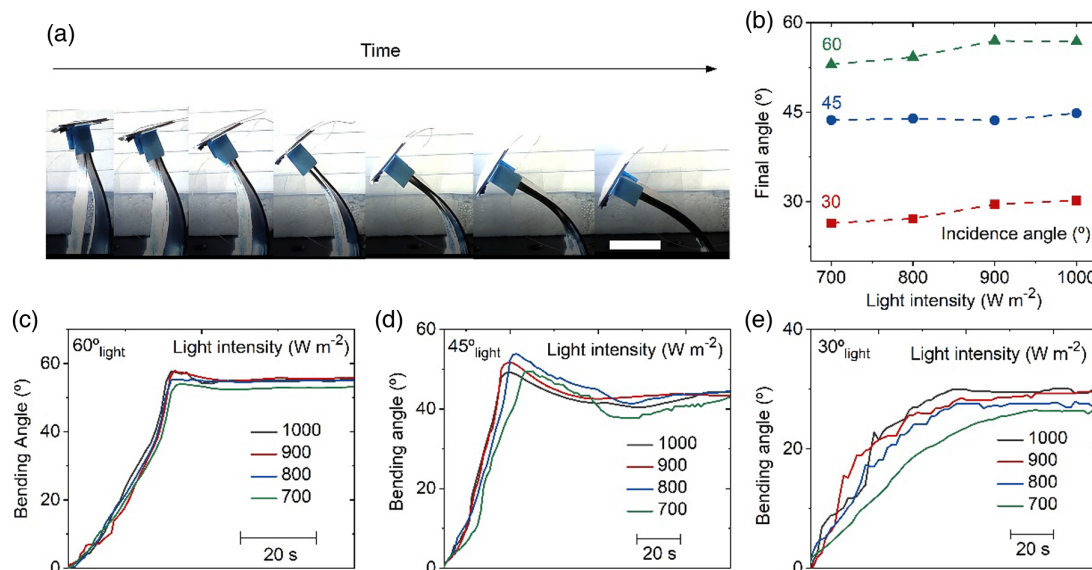


**Figure 2.** a) Optical images of the phototropic system during bending. Scale bar represents 1 cm. b) Final bending angle of the phototropic system versus light intensity at different incidence angles. c–e) Time-dependent bending angle of the phototropic system at different light intensities at  $60^\circ$ ,  $45^\circ$ , and  $30^\circ$  incidence angle, respectively.

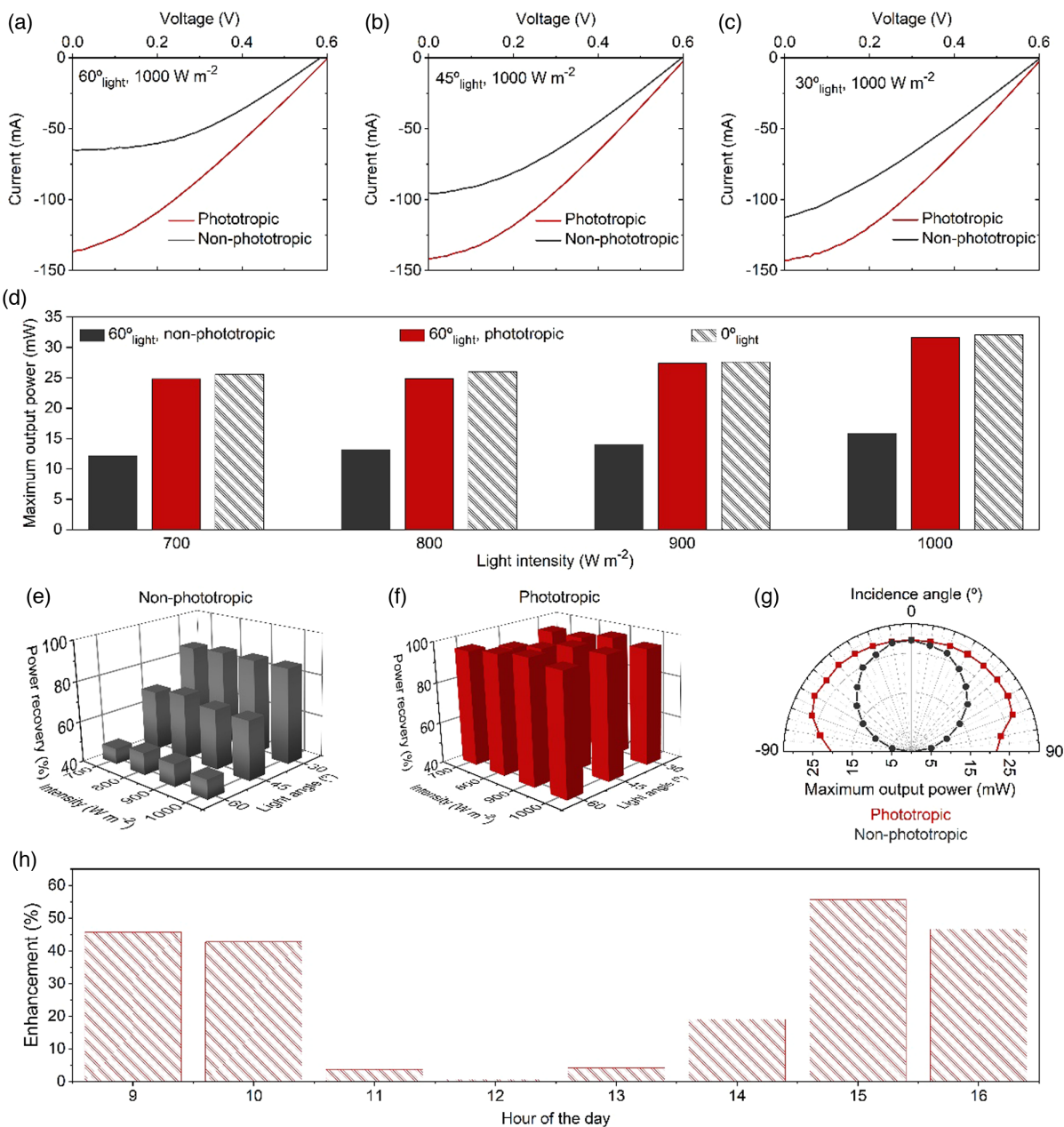


**Figure 3.** a–c) *I*–*V* curves of the phototropic solar panel and the nonphototropic solar panel illuminated with 60°, 45°, and 30° light, respectively. d) Maximum output powers of the phototropic solar panel and nonphototropic solar panel illuminated with 60° and 0° incidence light. e, f) Power recovery percentage, with respect to 0° incidence, of the phototropic solar panel and the nonphototropic solar panel, respectively. g) Maximum output power of the phototropic solar panel and the nonphototropic solar panel under 1000 W m<sup>-2</sup> illumination at different incident angles. h) Maximum output power enhancement of the phototropic solar panel at different hours of the day relative to the nonphototropic solar panel.

compared with that of 0° light illumination of that intensity. Compared with the phototropic device, the power output of the nonphototropic device at 60° is approximately half of the former, consistent with the cosine relationship shown in Figure 1c. The tracking solar panel illuminated with 60° light gave a 95.7–99.2% power output compared with 0° light of the same intensity. Power recovery percentage (defined as the device output power with angled light divided by that with vertical light) of

the nonphototropic device (Figure 3e) and phototropic device (Figure 3f) at various light intensity and angles are also tested. Regardless of the light intensity, the nonphototropic device can recover around 86%, 70%, and 50% of light at 30°, 45°, and 60° incidence angle, respectively, consistent with the cosine relationship. The phototropic device can recover more than 95% of the power for almost all combinations of the incidence angle and intensity, showing its significant strength of recovering OEL,

even at light intensity lower than 1 sun ( $1000 \text{ W m}^{-2}$ ). Incidence angle-dependent power recovery was also examined (Figure 3g). For the phototropic devices, the “front-bending” ( $0\text{--}90^\circ$ ) and “back-bending” ( $-90^\circ$  to  $0^\circ$ ) have similar power output, showing symmetric performance and the ability to track light across the entire hemisphere above the horizon. At nearly all incidence angles, the phototropic device can produce larger power output than the nonphototropic counterpart. At the large incidence angles of  $70^\circ$  and  $80^\circ$ , the phototropic device can generate 2.85 and 4.47 times the power of the nonphototropic device, respectively. At an incidence angle of  $90^\circ$  where the nonphototropic device can barely get any power output, the phototropic device could still generate power comparable with the nonphototropic device illuminated at  $40^\circ$ . All results were indicating that the phototropic device can effectively recover OEL.

## 2.4. Outdoor Experiment of the Solar Panel Phototropic Device

An outdoor experiment further demonstrated the ability of the solar panel phototropic device to capture more power (Figure 3h and Figure S9, Supporting Information) compared with the nonphototropic device. The  $I$ - $V$  curves of the

phototropic solar nonphototropic devices are recorded from 9 a.m. to 4 p.m. on a winter day. At 3 p.m., the phototropic device delivered a 55% higher output compared with the nonphototropic device, which is the result of the combination of a relatively large incidence angle and large light intensity. At larger incidence angles, at 9 a.m. or 4 p.m., the enhancement is slightly decreased to around 45%. Although the incident angle is larger, the light intensity is reduced, so bending may not fully lead to the exact alignment with the incident light. Still, for such a device with low-cost components and simple fabrication, it is remarkable that it can show a real-life application with enhanced power recovery. The bimorph design helps with the large actuation angle despite the relatively low temperature and sunlight intensity during winter, and the double-leg support design allows it to stand firmly against the wind and other air turbulence that might be present in the outdoor environment.

## 2.5. SVG Experiments of the Device

To demonstrate the versatility of the phototropic system proposed in this work, a phototropic SVG device (Figure 4a; Figure S10, Supporting Information; see also Experimental

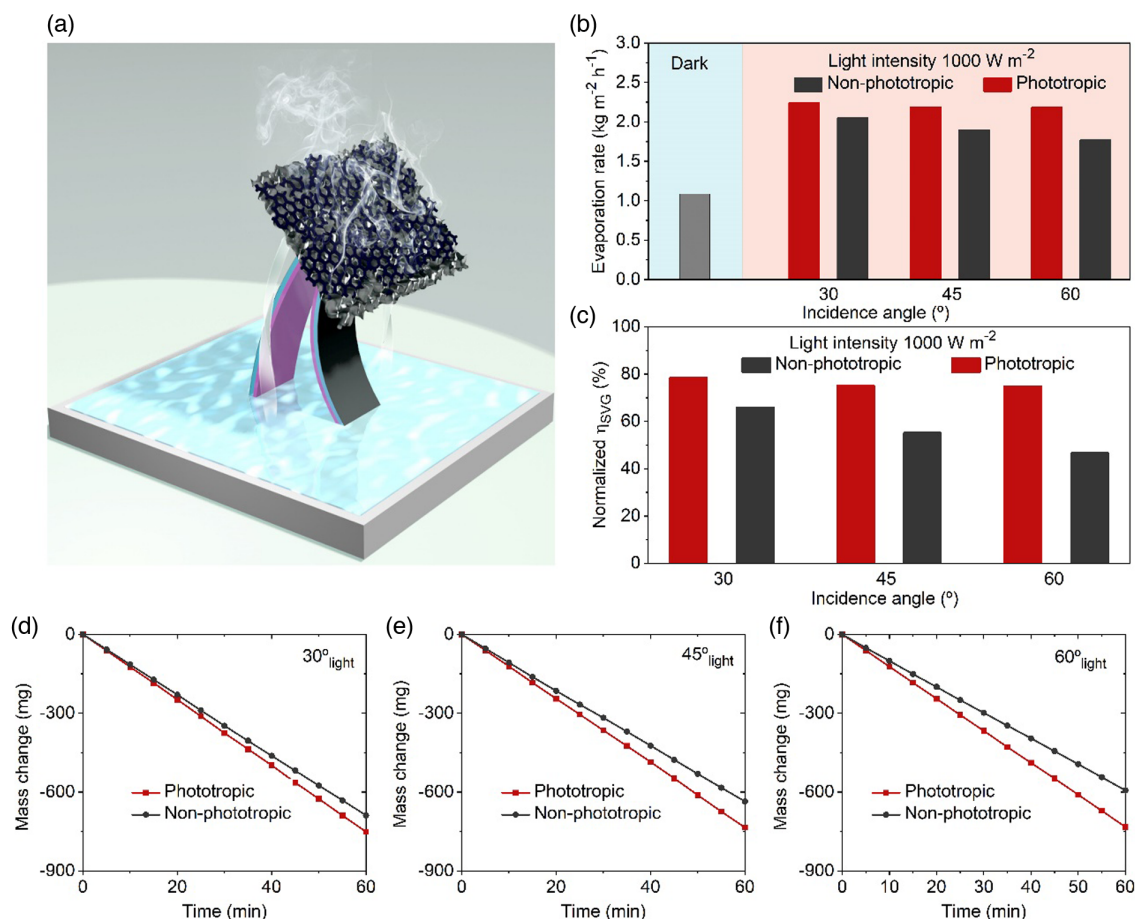


**Figure 4.** a) Schematic illustration of the phototropic SVG device. b) Evaporation rate of the phototropic SVG device and the nonphototropic SVG device in dark as well as under  $1000 \text{ W m}^{-2}$  illumination at different incident angles. c) Normalized SVG efficiencies of the phototropic SVG device and the nonphototropic SVG device. d–f) Mass change in the phototropic SVG device and the nonphototropic SVG device illuminated with  $30^\circ$ ,  $45^\circ$ , and  $60^\circ$  light, respectively.

Section) was made to carry out SVG experiments. Harvesting solar energy for steam generation is an emerging field for water purification and desalination. The technology uses a photothermal absorber layer at water–air interface to efficiently convert solar energy to thermal energy for water to evaporate. We utilized the LCE tracking device to overcome the OEL issues, enabling the enhanced harvesting of solar energy and increased production of purified water. To construct the device, Kimwipes and graphene oxide (GO) were used as the water carrier and photothermal absorber, respectively. The mass change in the device over time when illuminated with 30°, 45°, and 60° light was recorded (Figure 4d–f, respectively). Linear changes in mass were observed, indicating fast phototropic response of the device. The dark evaporation rate and the illuminated evaporation rates were calculated for the phototropic and nonphototropic SVG devices (Figure 4b). Then, The normalized SVG efficiencies were calculated according to the definition from Qian *et al.*<sup>[1]</sup> with the maximum evaporation rate value from Li *et al.*<sup>[20]</sup> (Figure 4c). The enhancements of the phototropic device, compared with the nonphototropic ones, are 20%, 36%, and 61% for 30°, 45°, and 60° light, respectively. The relatively low enhancements (for 60°, the enhancement should be 100% as previously discussed) and the low overall SVG efficiencies (only 80%, compared with 95% and above which are commonly seen in studies) could result from underoptimized photothermal converter and thermal insulation. Nevertheless, this result has demonstrated that the phototropic SVG device is fully capable to enhance the light power recovery of oblique incidence light and thus enhance the SVG efficiency.

### 3. Conclusion

In this work, we demonstrated a low-cost, easy-to-fabricate, unconcentrated sunlight-driven phototropic system exhibiting versatile usage. It features fast response and large bending angles, which benefits its ability to recover the OEL. Remarkably, it can still achieve large bending angles even when illuminated with sunlight of less than 1 sun intensity (700, 800, and 900 W m<sup>-2</sup>). This phototropic system demonstrated the ability to enhance the power output of solar panels via OEL recovery. Compared with nonphototropic devices, the phototropic device can generate 2, 2.85, and 4.47 times power harvesting at 60°, 70°, and 80° incidence angles, respectively. At an incidence angle of 90°, where the nonphototropic device has zero power output, the phototropic one can still generate power similar to the nonphototropic device illuminated at 40°. During an outdoor experiment with low temperatures, low light intensity, and wind, it can still generate as much as 55% higher power than the stationary solar panel. The versatile design of the system can also be used in SVG by simply substituting the solar panel on top with a water carrier containing embedded photothermal absorber. Compared with the nonphototropic device, it can enhance the SVG efficiency up to 61%, demonstrating its ability to reorient toward light and recover the OEL. Overall, the ability to directly utilize unconcentrated sunlight, large bending, and fast response showcases its unique strengths among phototropic systems. For real application, fast response is particularly useful in utilizing intermittent light conditions such as partial cloudy days where

the light will shine intermittently due to moving clouds. This design provides a new strategy for the future study and industrialization of artificial phototropic systems. The design is also compatible with solar concentrators, which opens future investigations for improved speed and bending in the system.

### 4. Experimental Section

**Synthesis of LCE:** 1,4-Bis[4-(3-acryloyloxypropoxy)benzoyloxy]-2-methylbenzene (Shijiazhuang Sdyano Fine Chemical, Co., Ltd., 2.5 g), toluene (AR(ACS), Avantor Performance Materials, 0.775 g), and 2-hydroxy-4'-(2-hydroxyethoxy)-2-methylpropiophenone (98%, Sigma-Aldrich, 0.015 g) were mixed in a vial and heated to 60 °C to dissolve. In a separate vial, 2,2'-(ethylenedioxy)diethanethiol (95%, Sigma-Aldrich, 0.48 g), pentaerythritol tetrakis(3-mercaptopropionate) (>95%, Sigma-Aldrich, 0.096 g), and 2.63 g of the aforementioned RM257 solution were added. This mixture was stirred at 800 rpm and 2% dipropylamine (99%, Sigma-Aldrich) in toluene solution (330 μL) was added dropwise. The mixture was then poured into a mold (spacer 0.8 mm) fabricated with plastic board support with PTFE tape (Impresa) and put in room temperature overnight. The mixture was then removed from the mold and put in an 80 °C vacuum oven (XLH-6020) overnight. Then the LCE film was stretched to 140–150% of its original length and illuminated with UV for 20 min (Dymax BlueWave 200 Rev. 3.0) while keeping it stretched.

**UV–vis Spectroscopy:** The transmittance spectrum was recorded using a Shimadzu UV-3101PC UV–vis–NIR scanning spectrophotometer. The reflectance spectrum was recorded using a Shimadzu MPC-3100 Multi-Purpose Large-Sample Compartment with an integrating sphere. Barium Sulfate (022-00425, Wako Pure Chemical Industries) was used as the 100% reflectance standard.

**Fabrication of the Phototropic and the Nonphototropic Solar Panel Device:** PVC tape (Topzone) was adhered to one side of the LCE. On the other side of the LCE Sharpie ink was homogeneously applied. Tape was used to fix the LCE legs on a glass substrate and solar panel on top of the device. For nonphototropic device, the solar panel was simply put horizontally on the bench. Silver wire (99.95% pure, 0.005" diameter, Surepure Chemetals) was used to connect the solar panel to Keithley 2450 Sourcemeter, which was used to record the *I*–*V* curve of the solar panel.

**Solar Cell Information:** The solar cell dimensions are 2.8 cm × 1.2 cm with a weight of 156 mg. *V*<sub>oc</sub> = 0.6 V, *J*<sub>sc</sub> = 0.14 A, filling factor = 54.4%, efficiency 9.5%.

**Outdoor Experiment:** The experiment was conducted on December 19, 2019 at 34°04'07.6"N 118°26'33.5"W, Los Angeles, from 9 a.m. to 4 p.m. Pacific Daylight Time. Temperature is 60–65 °F. Both the phototropic and nonphototropic device were preoriented so that the sun at 12 p.m. Pacific Daylight Time is directly above the solar panel. For phototropic devices, the bending direction also matches the sun trajectory of the day. Silver wire and Keithley are the same as previous.

**Fabrication of the Phototropic and the Nonphototropic SVG Device:** The ink/LCE/tape assembly was the same as previously mentioned in the solar panel device part. Tape was used to fix the LCE legs on glass substrate and plastic board support on top of the device. Kimwipe (KIMTECH) was adhered to the plastic board support using Devcon. A plastic petri dish with deionized (DI) water (ELGA Purelab Ultra) was put underneath the glass substrate. The glass substrate covers most of the openings of the plastic petri dish to minimize evaporation through that location. Kimwipe strings were used to connect the water supply (in the plastic petri dish) and the Kimwipe on top of the device. Devcon was used to adhere the Kimwipes. Finally, GO solution (highly concentrated single layer GO [aqueous solution], Graphene Supermarket) was added dropwise on to the Kimwipe on top of the device. For nonphototropic devices, plastic board legs of the same length and position as the LCE legs were used. All the rest part of the device is the same.

**Solar Simulation Devices:** For all indoor experiments, a solar simulator (Asahi spectra HAL-320W solar simulator with TOU-1-31 telecentric

uniform illumination unit) was used to generate light. One sun checker (CS-40, Asahi spectra) was used to calibrate the light intensity. A protractor was used to calibrate the light angle.

## Supporting Information

Supporting Information is available from the Wiley Online Library or from the author.

## Acknowledgements

Y.Y. and Y.Z. contributed equally to this work. This work was supported by Air Force Office of Scientific Research (AFOSR) Grant FA9550-17-1-0311, AFOSR award FA9550-18-1-0449, Office of Naval Research (ONR) Award N000141712117, ONR Award N00014-18-1-2314, the Hellman Fellows Funds, and the UCLA Faculty Career Development Award from the University of California, Los Angeles. X.H. is a Canadian Institute for Advanced Research Azrieli Global Scholar in the Bio-inspired Solar Energy Program.

## Conflict of Interest

The authors declare no conflict of interest.

## Keywords

artificial phototropism, liquid crystal elastomers

Received: October 15, 2020  
Revised: November 13, 2020  
Published online:

- [1] X. Qian, Y. Zhao, Y. Alsaïd, X. Wang, M. Hua, T. Galy, H. Gopalakrishna, Y. Yang, J. Cui, N. Liu, M. Marszewski, L. Pilon, H. Jiang, X. He, *Nat. Nanotechnol.* **2019**, *14*, 1048.
- [2] H. S. Atamian, N. M. Creux, E. A. Brown, A. G. Garner, B. K. Blackman, S. L. Harmer, *Science (80-)*. **2016**, *353*, 587.
- [3] I. A. Mashaly, K. Nassar, S. I. El-Henawy, M. W. N. Mohamed, O. Galal, A. Darwish, O. N. Hassan, A. M. E. Safwat, *Renew. Energy* **2017**, *109*, 202.
- [4] Motion Free Optical Tracking, <https://www.renkube.com/> (accessed: August 2020).
- [5] Smartflower, <https://smartflower.com/> (accessed: August 2020).
- [6] Solar Sunflower, <https://arstechnica.com/science/2015/08/the-solar-sunflower-harnessing-the-power-of-5000-suns/> (accessed: August 2020).
- [7] Gemasolar, <https://torresolenergy.com/en/gemasolar/> (accessed: August 2020).
- [8] Ivanpah, <https://www.energy.gov/lpo/ivanpah> (accessed: August 2020).
- [9] C. Li, Y. Liu, X. Huang, H. Jiang, *Adv. Funct. Mater.* **2012**, *22*, 5166.
- [10] B. Baytekin, S. D. Cezan, H. T. Baytekin, B. A. Grzybowski, *Soft Robot.* **2018**, *5*, 93.
- [11] J. Han, W. Jiang, D. Niu, Y. Li, Y. Zhang, B. Lei, H. Liu, Y. Shi, B. Chen, L. Yin, X. Liu, D. Peng, B. Lu, *Adv. Intell. Syst.* **2019**, *1*, 1900109.
- [12] L. Liu, M. del Pozo, F. Mohseninejad, M. G. Debije, D. J. Broer, A. P. H. J. Schenning, *Adv. Opt. Mater.* **2020**, *8*, 2000732.
- [13] M. Amjadi, M. Sitti, *ACS Nano* **2016**, *10*, 10202.
- [14] H. Cheng, F. Zhao, J. Xue, G. Shi, L. Jiang, L. Qu, *ACS Nano* **2016**, *10*, 9529.
- [15] K. W. Böer, *Sol. Energy* **1977**, *19*, 525.
- [16] T. J. White, S. V. Serak, N. V. Tabiryan, R. A. Vaia, T. J. Bunning, *J. Mater. Chem.* **2009**, *19*, 1080.
- [17] K. M. Lee, H. Koerner, R. A. Vaia, T. J. Bunning, T. J. White, *Macromolecules* **2010**, *43*, 8185.
- [18] H. M. D. Bandara, S. C. Burdette, *Chem. Soc. Rev.* **2012**, *41*, 1809.
- [19] S. Sun, S. Liang, W. C. Xu, G. Xu, S. Wu, *Polym. Chem.* **2019**, *10*, 4389.
- [20] X. Li, G. Ni, T. Cooper, N. Xu, J. Li, L. Zhou, X. Hu, B. Zhu, P. Yao, J. Zhu, *Joule* **2019**, *3*, 1798.